ALMA reveals bright circumgalactic emission and a biconical outflow in z ∼ 6.4 quasar PSOJ183+05

Manuela Bischetti,[1,2] Chiara Feruglio,[2,3] Stefano Carniani,[4] Valentina D'Odorico,[2,3,4]
Francesco Salvestrini,[2] and Fabrizio Fiore[2,3]

[1]*Dipartimento di Fisica, Universitá di Trieste, Sezione di Astronomia, Via G.B. Tiepolo 11, I-34131 Trieste, Italy*
[2]*INAF - Osservatorio Astronomico di Trieste, Via G. B. Tiepolo 11, I–34131 Trieste, Italy*
[3]*IFPU - Institut for fundamental physics of the Universe, Via Beirut 2, 34014 Trieste, Italy*
[4]*Scuola Normale Superiore, Piazza dei Cavalieri 7, I-56126 Pisa, Italy*

Submitted to ApJL

ABSTRACT

Understanding gas flows between galaxies and their surrounding circum-galactic medium (CGM) is crucial to unveil the mechanisms regulating galaxy evolution, especially in the early Universe. However, observations of the CGM around massive galaxies at $z > 6$ remain limited, particularly in the cold gas phase. In this work, we present multi-configuration ALMA observations of [CII]$\lambda158,\mu$m and millimetre continuum emission in the $z \sim 6.4$ quasar PSOJ183+05, to trace the cold CGM and investigate the presence of outflows. We find clumpy [CII] emission, tracing gas up to a ~ 6 kpc radius, consistent with the interface region between the interstellar medium (ISM) and CGM. The [CII] kinematics shows a rotating disk and a high-velocity, biconical outflow extending up to 5 kpc. The inferred mass outflow rate is $\dot{M}_{\rm of} \sim 930$ M⊙ yr^{-1}, among the highest at $z > 6$, and comparable to the star-formation rate. These findings suggest that quasar-driven outflows can rapidly transfer energy and momentum to the CGM, without immediately quenching star formation in the host galaxy ISM. This supports a delayed feedback scenario, in which outflows reshape CGM conditions and regulate future gas accretion over longer timescales. Combining high-resolution and sensitive ALMA data with observations from JWST and MUSE will be crucial to map the CGM across its different phases and build a comprehensive picture of the baryon cycle in the first massive galaxies.

Keywords: galaxies: high-redshift, quasars: emission lines, galaxies: evolution, techniques: interferometric, galaxies: halos, galaxies: kinematics and dynamics

1. INTRODUCTION

The acquisition, ejection, and recycling of gas are fundamental processes driving galaxy evolution. The primary site of these gas flows is the circum-galactic medium (CGM), a region extending beyond a galaxy's stellar distribution up to its virial radius and beyond. CGM serves as a major baryon reservoir, providing inflows of fuel for star-formation to the insterstellar medium (ISM), and acting as the immediate destination for outflows driven by feedback processes within galaxies (Tumlinson et al. 2017). Attaining a complete picture

Corresponding author: M. Bischetti
manuela.bischetti@units.it

of how galaxies evolve is thus hampered by our incomplete knowledge of the cycle of baryons between ISM and CGM. This issue is particularly relevant for the first massive ($\gtrsim 10^{10}$ M$_\odot$) galaxies, which formed 0.5-1 Gyr after the Big Bang ($z > 6$). According to the hierarchical scenario of structure formation (e.g. Springel et al. 2005), these galaxies trace the densest regions of the Universe which were the first to collapse, and thus represent a relevant population of progenitors of the most massive galaxies that we observe in today's Universe.

The first pioneering studies of CGM halos relied on absorption features of the intervening gas in quasar spectra, and provided a robust description of the average CGM conditions from the first Gyr (e.g. Adelberger et al. 2005; Turner et al. 2014; Prochaska et al. 2014; Kashino et al. 2023; Galbiati et al. 2023). However,

these probes precluded direct constraints on the three-dimensional structure of the CGM. Spatially resolved observations of warm ($10^4 - 10^5$ K) CGM emitting gas have been performed with sensitive integral field unit (IFU) spectroscopy using the Multi Unit Spectroscopic Explorer (MUSE). Indeed, CGM halos have been seen routinely glowing in Lyα around massive galaxies hosting quasars up to $z > 6$ (Borisova et al. 2016; Farina et al. 2019). However, millimetre studies (mostly with the Atacama Large Millimetre Array, ALMA) have so far provided limited statistics on the detection of cold ($\lesssim 10^2$ K) CGM halos around a few massive galaxies and quasars at $z \sim 2$ (Cicone et al. 2021; Jones et al. 2023; Scholtz et al. 2023) and at $z > 6$ (Cicone et al. 2014; Lambert et al. 2023; Meyer et al. 2022; Bischetti et al. 2024). Studies based-on stacking have also provided conflicting results (Fujimoto et al. 2019; Novak et al. 2020). This scarcity of detections is likely due to most studies relying on observations not optimized to detect the diffuse CGM gas (e.g. see discussion in Carniani et al. 2020).

Different scenarios have been proposed to explain the origin of CGM halos around the first massive galaxies, including stellar and black-hole driven outflows able to push metal-enriched gas to large scales (Costa et al. 2022; Pizzati et al. 2023). IFU spectroscopy with the James Webb Space Telescope (JWST) has opened a new window into detecting and mapping warm outflows using the [OIII]λ5008 Å emission line at $z > 6$ (e.g. Marshall et al. 2023). However, probing outflows in the cold gas phase immediately preceding star formation remains an observational challenge, and only a few detections have been reported (Maiolino et al. 2012; Feruglio et al. 2017; Bischetti et al. 2019a; Izumi et al. 2021a,b; Tripodi et al. 2022). This is likely due to the limited sensitivity of most millimetre observations, considering similar outflowing to total gas ratios as observed in the low redshift Universe (Bischetti et al. 2019b; Fluetsch et al. 2019).

In this work, we present ALMA observations of the [CII]λ158 μm emission line and millimetre continuum emission in the host galaxy of quasar PSOJ183+05 at $z \sim 6.4$ (Bañados et al. 2016) and CGM environment. We combined archival observations acquired with different antenna configurations, to boost the detectability of diffuse cold gas with respect to previous studies and, at the same time, map it with high resolution. The target of this work is a bright quasar with a bolometric luminosity $\log(L_{\rm Bol}/{\rm erg\ s}^{-1}) \simeq 47.2$, powered by a black hole with mass $\log({\rm M_{BH}/M_\odot}) \simeq 9.4$ (Farina et al. 2022; Mazzucchelli et al. 2023). PSOJ183+05 hosts a nuclear wind. A molecular outflow arising from the central kpc region has been detected in OHλ119 μm absorption by

Butler et al. (2023), with a median velocity of 530 km/s and an outflow rate of about 75-800 $M_\odot$ yr^{-1}. Previous [CII] studies of this source reported a bright emission, with a high luminosity $L_{\rm [CII]} \simeq 7 \times 10^9$ $L_\odot$ (Decarli et al. 2018) associated with a relatively compact disk dominated by rotation (Venemans et al. 2020; Neeleman et al. 2021).

2. ALMA OBSERVATIONS AND DATA ANALYSIS

We analyse archival ALMA observations of PSOJ183+05 targeting [CII] and band 6 continuum emission using CASA 6.4.0 software (McMullin et al. 2007). We consider observations of the [CII] $\nu_{\rm rest} = 1900.537$ GHz emission line, as acquired with three different antenna configurations, including a low angular resolution (project ID 2015.1.01115.S, $\sim$ 1.1 arcsec), a high angular resolution (ID 2016.1.00544.S, $\sim$ 0.12 arcsec), and an intermediate resolution (ID 2019.1.01633.S, $\sim$ 0.3 arcsec) dataset.

Combining visibilities acquired from different antenna configurations allows us to maximise the sensitivity to possible extended [CII] emission, while keeping a reasonably good angular resolution. We did not combine an additional low-resolution dataset (ID 2021.1.01082.S, $\sim$ 1.3 arcsec) available on the archive, whose spectral coverage is limited to velocities $|v| \lesssim 1000$ km s^{-1} with respect to the [CII] line, introducing high uncertainty in the modelling and subtraction of the continuum emission.

Visibilities were calibrated using the standard calibration provided by the ALMA observatory and the default phase, bandpass and flux calibrators. We merged the visibilities from the three datasets using CASA (version 6.6.5) task *concat*. We created a continuum map (Figure 1a) by averaging visibilities over all spectral windows, covering the observed frequencies $237.7 - 242.8$ and $252.7 - 257.9$ GHz, and excluding the spectral range covered by [CII]. To model and subtract the continuum emission from the line, we combined the adjacent spectral windows in the baseband containing [CII] and performed a fit in the uv plane to channels with $|v| > 1000$ km s^{-1}, using a first-order polynomial continuum. A continuum-subtracted datacube was created using CASA task *tclean*, with the *hogbom* cleaning algorithm in non-interactive mode, a threshold equal to two times the rms sensitivity and a natural weighting of the visibilities. We adopted a 30 km s^{-1} channel width. The resulting synthesized beam for the spectral window including [CII] is 0.13×0.12 arcsec^2, the rms sensitivity of the [CII] datacube is $\sigma_{30} = 0.095$ mJy beam^{-1} for a 30 km s^{-1} channel width, and the rms sensitivity of the continuum map is $\sigma_{\rm cont} = 6.6$ μJy beam^{-1}.

Table 1. Properties of PSOJ183+05.

RA	12:12:26.974
Dec	+05:05:33.540
$z_{\rm [CII]}$	6.4388±0.0004
$S_{\rm cont}$ [mJy]	3.53±0.04
$S_{\rm [CII]}$ [Jy km s^{-1}]	10.1±0.25
$L_{\rm [CII]}$ [10^{10}L$_\odot$]	1.09±0.03
$M_{\rm atom}$ [10^{10}M$_\odot$]	1.51±0.04
[CII] outflow	
$S_{\rm [CII]}$ [Jy km s^{-1}]	3.64±0.52
L'$_{\rm [CII]}$ [10^{10}L$_\odot$]	0.39±0.05
$M_{\rm atom}$ [10^{10}M$_\odot$]	0.54±0.04
$\langle v_{\rm mom1} \rangle$ [km s^{-1}]	-30 ± 65
$\langle v_{\rm max} \rangle$ [km s^{-1}]	790 ± 110
$r_{\rm of}$ [kpc]	$0.3 - 4.8$
$\dot{M}_{\rm of}$ [M$_\odot$ yr^{-1}]	930^{+330}_{-290}

NOTE—RA, Dec refer to the peak of the 237.7-257.9 GHz continuum. $\langle v_{\rm mom1} \rangle$ and $\langle v_{\rm max} \rangle$ are the flux weighted velocity shift and maximum velocity of the outflow, respectively (Fig. 3). Uncertainties correspond to a 68% confidence level except for $\dot{M}_{\rm of}$ (see Sect. 4.1).
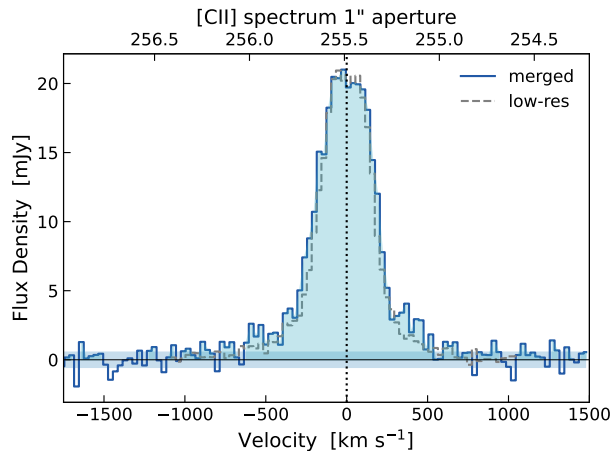
Figure 1. [CII] spectrum extracted from a circular 1 arcsec aperture (blue histogram), similar to the spatial extent of the broad [CII] emission component mapped in Fig. 3. The presence of blue/redshifted wings reaching velocities of ± 1000 km s^{-1} can be observed. The wings are also visible in the spectrum extracted with the same aperture in the low-resolution dataset 2021.1.01082.S (normalized for comparison to the peak of the spectrum of the combined dataset). The horizontal shaded region corresponds to the $\pm 1\sigma$ noise level, calculated as $\sigma_{30}\sqrt{N}$, where N is the number of the independent ALMA beams in the extraction aperture.

We performed a pixel-by-pixel spectral decomposition of [CII] emission detected at $> 3\sigma_{30}$ in the continuum-subtracted datacube. To reproduce the [CII] emission line profile in PSOJ183+05 (Fig. 1), we considered a model with two Gaussian components: a main one with FWHM< 500 km s^{-1} to account for the systemic [CII] emission, based on previous line width measurements (Venemans et al. 2020), and a second broad Gaussian with a FWHM> 500 km s^{-1}, to account for possible high-velocity wings in the line profile. The amplitude of this broad component is limited at maximum 20% of the systemic component, consistently with the most prominent [CII] wings observed in low-z active galaxies and high-z quasars (Maiolino et al. 2012; Bischetti et al. 2019a; Fluetsch et al. 2019).

The resulting velocity-integrated intensity ($0^{\rm th}$ moment), velocity ($1^{\rm st}$ moment) and velocity dispersion ($2^{\rm nd}$ moment) maps associated with the total [CII] emission in PSOJ183+05 are shown in Fig. 2. Moment maps associated with the high-velocity [CII] emission are displayed in Fig. 3.

3. CONTINUUM AND [CII] EMISSION

ALMA observations of the $\sim 240 - 255$ GHz continuum in PSOJ183+05, detected at $\sim 160\sigma_{\rm cont}$ level, reveal that the bulk of the emission is associated with dust in the host galaxy ISM (Fig. 2a). By fitting the continuum map with a 2D Gaussian profile, we infer a deconvolved size of $(0.23 \pm 0.01) \times (0.21 \pm 0.01)$ arcsec^2, corresponding to about 1.3×1.2 kpc^2. This compact size is consistent with that previously measured for PSOJ183+05 by Venemans et al. (2020) using 0.2 arcsec ALMA observations, and similar to those reported for the millimeter continuum in the host galaxies of most $z \gtrsim 6$ quasars (e.g. Feruglio et al. 2018; Tripodi et al. 2024a). It is also consistent with the region in which the bulk of the stellar mass is likely located. Indeed, the dashed circle in Fig. 2 corresponds to the effective radius measured by the Near-Infrared Camera (NIRCam) on board of JWST for the stellar distributions in $z \gtrsim 6$ quasars (e.g. Ding et al. 2023; Stone et al. 2023, 2024; Yue et al. 2024), powered by black holes with similar $L_{\rm Bol}$ and $M_{\rm BH}$ to PSOJ183+05.

The [CII] emission in PSOJ183+05, detected at $\sim 50\sigma_{\rm [CII]}$ level, spans an angular region of almost 2×2 arcsec^2 around the quasar location (Fig. 2b) and appears to be clumpier than the continuum emission (e.g. Venemans et al. 2019; Zanella et al. 2024). We measure a [CII] luminosity (using Eq. 1 in Solomon & Vanden Bout (2005)) $L_{\rm [CII]} \simeq 1.1 \times 10^{10}$ L$_\odot$ (Table 1), that is a factor of about two higher than previous measurements in this source (Decarli et al. 2018; Venemans et al. 2020). By imaging the individual datasets following the approach in 2, we verified that this is due to the increased sensitivity to the extended [CII] emission provided by
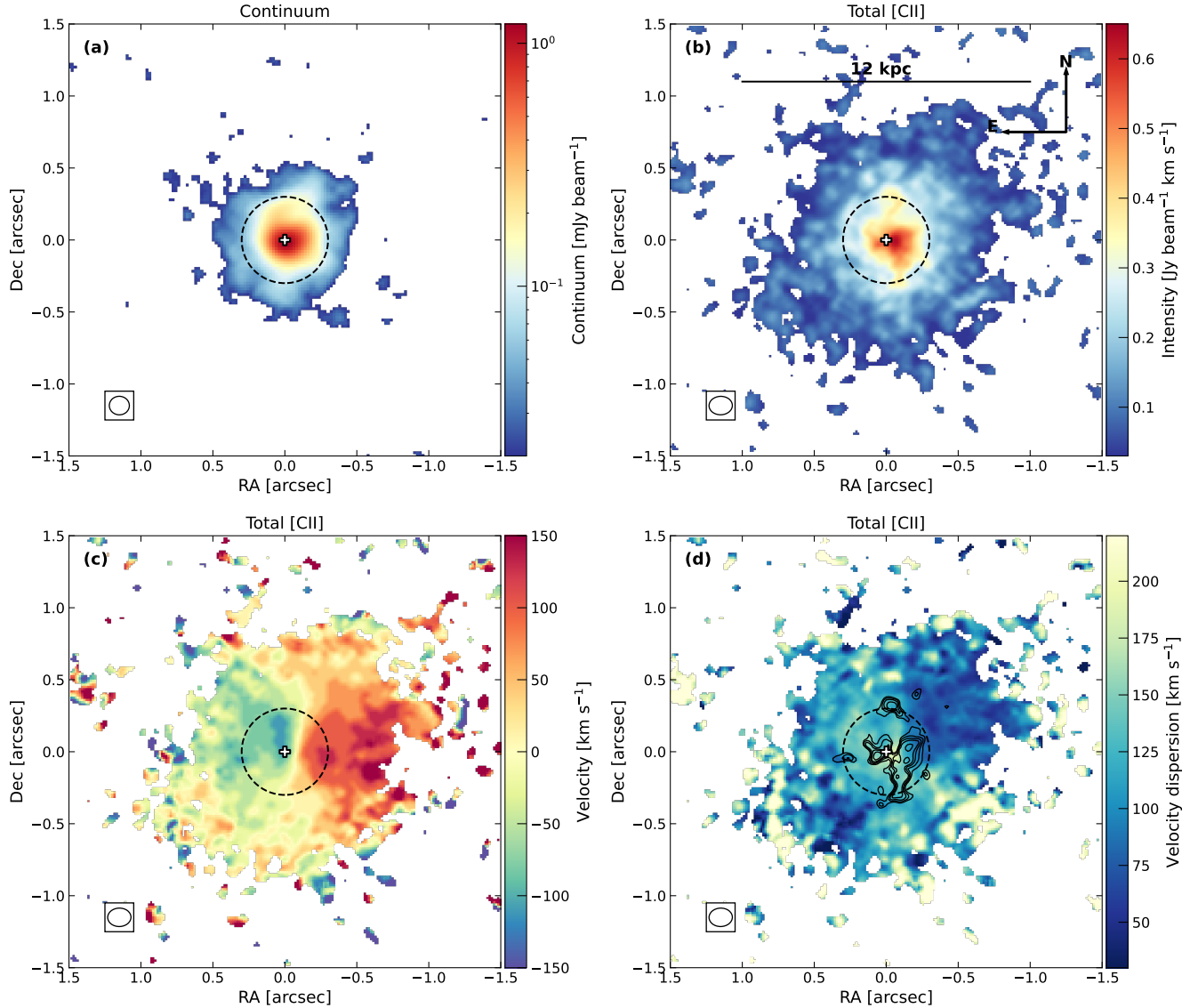
Figure 2. (a): Map of continuum emission detected at $> 3\sigma_{\rm cont}$ in the host galaxy of PSOJ183+05. Quasar location, identified as the peak of the ALMA continuum, is shown by the cross. (b): Velocity-integrated intensity map of [CII] emission detected $> 3\sigma_{\rm [CII]}$. (c): [CII] Velocity map. (d) [CII] velocity dispersion, showing a biconical region oriented along the SE-NW direction with high $\sigma_{\rm vel} \sim 150$ km s^{-1}. Contours highlight the location of the high-velocity [CII] emission with intensity > 0.02 Jy beam^{-1} km s^{-1} (Fig. 2 top panel). The displayed region of 3×3 arcsec^2 corresponds to the field of view covered by JWST/NIRSpec IFU. The dashed circle indicates the size of the stellar distribution measured by JWST/NIRCam observations in the host-galaxies of $z \sim 6$ quasars (Sect. 4.2). The white ellipse shows the ALMA beam.

the combined dataset. By fitting the [CII] map with a 2D Gaussian profile, we find a deconvolved FWHM size of $(0.83 \pm 0.04) \times (0.75 \pm 0.03)$ arcsec^2, corresponding to about 4.7×4.2 kpc^2. However a single component Gaussian fit results in bright residuals (at $\sim 15\sigma_{\rm [CII]}$ level, where $\sigma_{\rm [CII]} = 0.015$ Jy beam^{-1} km s^{-1} is the rms of the moment 0 map) in the central 0.2 arcsec, and negative residuals at larger distance from the nucleus, suggesting two distinct [CII] emitting components. No significant residuals are obtained by fitting a two Gaus-

sians model: this results in a compact component, with a deconvolved major FWHM size of (0.26 ± 0.03) arcsec (~ 1.5 kpc), consistent with the continuum size, plus an extended component with a FWHM of (1.03 ± 0.04) arcsec, corresponding to about 5.8 kpc. The size of this extended component is a factor of two-to-three larger than the [CII] sizes typically measured using high-resolution ($\lesssim 0.2$ arcsec, Bischetti et al. 2018; Venemans et al. 2020; Neeleman et al. 2023) ALMA observations, while it is among the largest sizes reported using moderate or low-

resolution ALMA observations, which are more sensitive to [CII] emission on scales $\gg 1$ kpc (Decarli et al. 2018; Fudamoto et al. 2022; Wang et al. 2024). The extended [CII] also reaches significantly further out than the stellar distribution measured by JWST (Fig. 2b), suggesting that we are probing [CII] emission arising from the interface region between ISM and CGM.

The [CII] velocity map in PSOJ183+05 (Fig. 2c) shows a velocity gradient along the East-West direction, consistent with the ISM rotation identified by Neeleman et al. (2021), although deviations are present in the North and mostly in the South regions at ~ 3 kpc from the quasar. This may be due to radial gas flows: either inflows close to the minor rotation axis, with a velocity component along the line of sight of ~ 40 km s^{-1}, or outflowing gas whose presence is revealed by high-velocity [CII] emission (Sect. 4.1). The [C II] velocity dispersion is generally moderate ($\sigma_{\rm v} \lesssim 100$ km s^{-1}), consistent with the [CII] clumps being formed through violent disk instabilities, similarly to what observed in other high-z galaxies and quasars (e.g Förster Schreiber et al. 2018; Inoue et al. 2016). An increased $\sigma_{\rm v} \sim 150-200$ km s^{-1} is observed in a biconical region centered on the quasar and extending out to ~ 5 kpc in the North-East to South-West direction. We interpret this increased dispersion as due to the interaction of a [CII] outflow with the ISM and CGM of the host galaxy (Sect. 4.1), similarly to what observed in low-redshift Seyferts and quasars, in which it has been possible to spatially disentangle outflow and disk components (Shimizu et al. 2019; Bischetti et al. 2019b; Zanchettin et al. 2023). Other processes such as galaxy interactions are disfavoured as (i) they cannot reproduce such a symmetric structure with high $\sigma_{\rm v}$ (e.g. Decarli et al. 2019), and (ii) we do not see a double peaked continuum or a disturbed [CII] morphology, which suggests that PSOJ183+05 is an isolated galaxy, in agreement with Venemans et al. (2020); Neeleman et al. (2021). We do not observe a decrease in velocity dispersion with increasing distance from the nucleus.

4. DISCUSSION

4.1. The [CII] outflow in PSOJ183+05

Fig. 3 shows the moment $0^{\rm th}$, moment $1^{\rm st}$ and $2^{\rm nd}$ maps associated with the broad ($FWHM > 500$ km s^{-1}) [CII] emission detected (at $\sim 8\sigma_{\rm [CII]}$ level) in the host galaxy of PSOJ183+05 (Sect. 2). We find this emission to be very clumpy (Fig. 3a) and distributed along the edges of the double cone in which the velocity dispersion of the total [CII] profile is increased (Fig. 3d), out to a distance of ~ 5 kpc from the quasar. The velocity shift of this broad component is relatively little ($-200 < v_{\rm mom1}^{\rm broad} < 200$ km s^{-1}), and the emission is
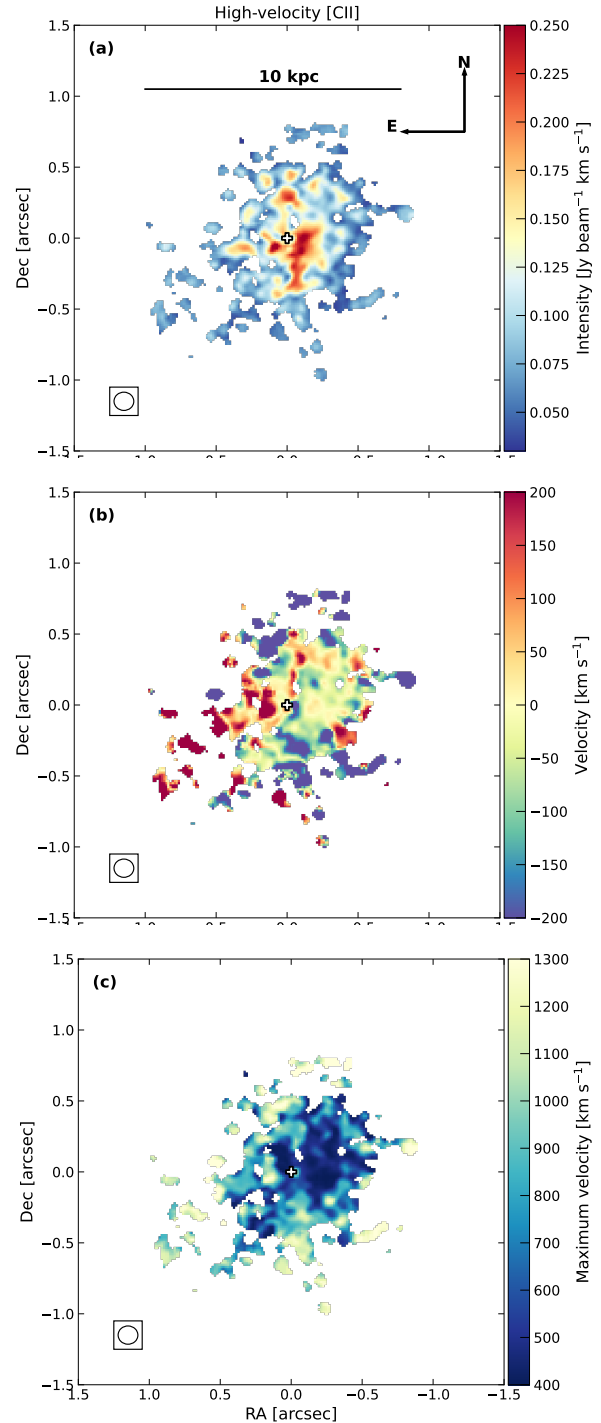
Figure 3. (a): Velocity-integrated intensity map associated with the broad [CII] emission (calculated as in Sect. 2). (b): Velocity map. (c) Maximum velocity of the [CII] outflow. The cross refers to the quasar location, corresponding to the peak of the ALMA continuum emission (Fig. 2a). The white ellipse shows the ALMA beam.

mostly redshifted(blueshifted) in the North-East(South-West) cone. We calculate the maximum velocity as

$v_{\max} = |v_{\mathrm{mom1}}^{\mathrm{broad}}| + 2\sigma_v^{\mathrm{broad}}$ (e.g. Bischetti et al. 2017; Fiore et al. 2017), where $\sigma_v^{\mathrm{broad}}$ is the velocity dispersion of the broad [CII] component. We find large values of $v_{\max}$ up to $\sim 1000 - 1200$ km s^{-1} (Fig. 3c). Such velocity is among the highest values measured in the [CII] profiles of local AGN and luminous quasars up to $z \gtrsim 6$ (Janssen et al. 2016; Bischetti et al. 2019a; Izumi et al. 2021a,b; Cicone et al. 2014), and indicates that the broad [CII] emission cannot be ascribed to bounded motion in the quasar host galaxy, but is instead associated with outflowing gas, likely accelerated by the supermassive black hole in the nucleus of PSOJ183+05. By performing a dynamical modelling of the [CII] kinematics in PSOJ183+05, Neeleman et al. (2021) reported a dynamical mass $M_{\mathrm{dyn}} \sim 1.3 \times 10^{11}$ M$_\odot$ in the inner 4 kpc around the quasar, which corresponds to an escape velocity of about 700 km s^{-1}. This implies that a significant fraction of the high-velocity [CII] emission is able to escape the potential well of the host galaxy and reach CGM scales.

From the moment 0th map of the high-velocity [CII] we calculate the outflowing atomic gas mass $M_{\mathrm{of}} \sim 5.4 \times 10^9$ M$_\odot$ in the assumption that most of [CII] is excited by photodissociation regions, according to Eq. (1) in (Hailey-Dunsheath et al. 2010), for a gas temperature $T = 200$K and a density significantly higher than [CII] critical density (Maiolino et al. 2012; Lagache et al. 2018; Bischetti et al. 2019a). This value corresponds to about 22% of the total atomic mass in PSOJ183+05. We calculate the mass-outflow rate at each radius r_{of} by applying the relation for a conical wind $\dot{M}_{\mathrm{of}} = \Omega \frac{M_{\mathrm{of}} v_{\max}}{r_{\mathrm{of}}} f$ (e.g. Bischetti et al. 2019b, 2017; Cicone et al. 2015), where Ω is the fractional solid angle spanned by the outflow bicone, and $f \simeq 1$ for a density profile scaling as r_{of}^{-2}, while $f \simeq 3$ for a constant density profile (e.g. Veilleux et al. 2017; Fiore et al. 2017). In our calculation, we calculate r_{of} for each pixel of the outflow map outside the central beam, while we consider r_{of} equal to the beam radius in the central region. We consider $\Omega \sim 1/2$ (corresponding to a bicone opening angle of about 120 deg, Fig. 21) and $f \simeq 1$. The resulting total atomic mass outflow rate is $\dot{M}_{\mathrm{of}} = 930_{-290}^{+330}$ M$_\odot$ yr^{-1}, where the uncertainty is dominated by that on the bicone opening angle (about ± 20 deg). This value is among the highest outflow rates reported in $z \gtrsim 6$ quasars (e.g. Tripodi et al. 2024a, and references therein). However, it is not much higher than the star-formation rate SFR $\sim 650 - 890$ M$_\odot$ yr^{-1} measured in the host galaxy of PSOJ183+05 based-on multi-frequency ALMA data sampling, and assuming a quasar contribution of 50% to dust heating (Decarli et al. 2023; Tripodi et al. 2024b; Duras et al. 2017).

The coexistence of powerful winds and high SFR has been often observed in the ISM of high-z quasar host galaxies (Feruglio et al. 2017; Bischetti et al. 2021; Lamperti et al. 2021; Vayner et al. 2024) and expected by cosmological simulations of early galaxy-evolution (e.g. Valentini et al. 2021), which is at odds with the expectations for an ejective feedback mode efficiently removing gas before it can fuel star formation. Instead, recent feedback theories have shifted toward a delayed feedback mode, primarily associated with processes occurring on CGM scale. The underlying idea is that the physical and kinematic conditions of the CGM may change during the feedback process, and these alterations may be the primary mechanism influencing further gas accretion and, consequently, reducing star formation (Costa et al. 2022; Barai et al. 2018). Such a scenario may be reasonably applied to PSOJ183+05, as the [CII] wind is able to reach and propagate its energy and momentum to the CGM gas on short timescale of a few million years, given the observed $v_{\max}$.
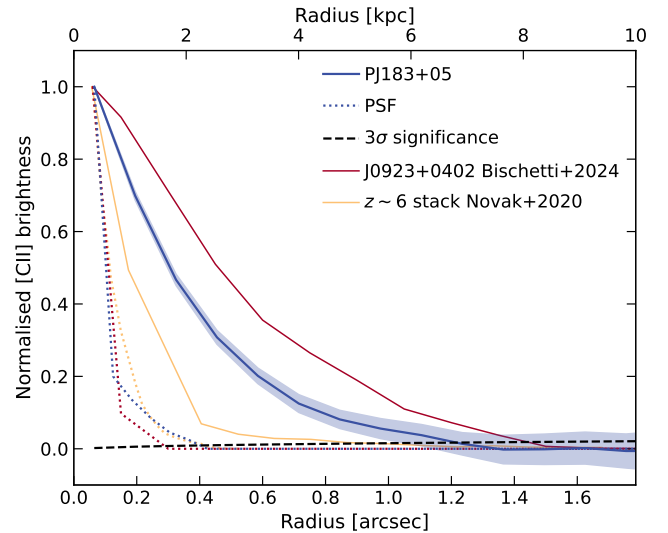
Figure 4. Brightness profile of the [CII] emission in PSOJ183+05 (blue solid curve), normalised to the central peak value, and associated 68% confidence level uncertainty (shaded area). The brightness profile associated with the ALMA point spread function (PSF) is shown by the dotted blue curve, while the dashed curve shows the profile associated with the 3σ level. We also show the profile for another $z \sim 6.6$ quasar (in a merger, red curve) showing extended [CII] emission from Bischetti et al. (2024) and the stacked profile of $z \sim 6$ quasar hosts by Novak et al. (2020), shown by the yellow curve.

4.2. Bright CGM emission and feedback

The ALMA observations of PSOJ183+05 presented in this work reveal the presence of a bright [CII] emis-

sion associated with the host galaxy ISM and CGM. [CII] is mostly a tracer of neutral atomic gas in photon-dominated regions (PDRs) around young stars but it can be also emitted from the partly ionised medium (Lagache et al. 2018; Casavecchia et al. 2024). However, the larger [CII] extent with respect to the millimetre continuum (Fig. 2a,b) suggests that a significant fraction of the extended [CII] emission may not arise from PDRs but may rather trace diffuse and ionised gas in the CGM.

This is supported by the fact that about 50% of the [CII] emission arises beyond a radius of 0.5 arcsec ($\simeq 2.8$ kpc), as it can be seen from Fig. 2b and the [CII] brightness profile of PSOJ183+05 showin in Fig. 4. The profile shows the average [CII] emission in circular annuli of 0.13" radius, calculated following the method described in Tripodi et al. (2022); Bischetti et al. (2024).

[CII] emission on scales beyond a few kpc has been previously detected by stacking samples of star forming galaxies at $z \gtrsim 5$, and in a few individual targets (Fujimoto et al. 2019, 2020; Ginolfi et al. 2020a; Herrera-Camus et al. 2021; Akins et al. 2022; Lambert et al. 2023). We find that size of the [CII] emission around PSOJ183+05 is about twice more extended than the stacked [CII] profile of $z \sim 6$ quasars by Novak et al. (2020). However, we note that the latter profile was based on high-resolution only observations which are not optimized to detect possible diffuse [CII] emission. Based-on ALMA simulated observations of $z > 6$ galaxies, Carniani et al. (2020) showed that a major fraction (about 50%) of the flux of the extended [CII] emission is not recovered when employing high-resolution observations only. By combining ALMA observations acquired with different antenna configurations, Bischetti et al. (2024) reported the discovery of a bright [CII] emission in the CGM of $z \sim 6.6$ quasar J0923+0402. The size of the [CII] emission in PSOJ183+05 is smaller than that of J0923+0402, although the latter is in a merging system, which might contribute to increase the region of [CII] emitting gas (Ginolfi et al. 2020b; Lambert et al. 2023).

Recent works have suggested a link between feedback and CGM halos around $z \sim 6$ star forming galaxies and quasars. Given the presence of a large-scale [CII] outflow in PSOJ183+05, such a scenario might explain its extended [CII] emission. Feedback via high-velocity outflows is able to displace gas beyond few kpc (Costa et al. 2019; Vito et al. 2022) and, at the same time, outflows can significantly contribute to gas heating via shocks (Appleton et al. 2013; Fujimoto et al. 2020; Pizzati et al. 2023). The multi-phase structure of the CGM gas depends on the fraction of photons reaching the CGM scales, which in turn depends on black-hole feedback clearing out the line of sights (Costa et al. 2022). Along the lines of sight with high escape fraction, the halo would be mostly ionized (e.g., Barai et al. 2018; Obreja et al. 2024), consistently with the Lyα halos frequently detected around high-z quasars (Borisova et al. 2016; Farina et al. 2019). If the global escape fraction remains relatively low (Stern et al. 2021), extended and bright [CII] halos are expected in massive halos such as those of $z \gtrsim 6$ quasars (Pizzati et al. 2023; Costa 2023).

5. CONCLUSIONS

This study has demonstrated that by combining ALMA datasets acquired with different antenna configuration, extended [CII] emission can be detected beyond ISM scale around the host galaxies of $z \gtrsim 6$ quasars. At the same time, mapping the cold gas emission with high-resolution allows to probe the gas kinematics on a broad range of scales (~ 500 pc to several kpc) and to investigate the presence of inflows and outflows and assess their impact on the large-scale gas reservoir. Several quasars and high-z galaxies have already been observed with multiple antenna configurations, which suggests that significant information on the CGM of massive early galaxies lies unexplored in the ALMA archive (e.g. see also Bischetti et al. 2024). However, the archival observations contains heterogenous observations in terms of angular resolution, sensitivity, and frequency coverage, which are not suited for a systematic study of CGM properties. This implies that complementary dedicated ALMA observations are needed.

To build a three-dimensional picture of the multi-phase CGM gas, ALMA information can be combined with that provided by MUSE and JWST for the warm ionized gas. In the case of PSOJ183+05, the high redshift implies that Lyα transition lies close to the edge of the MUSE spectral coverage, making a detection of diffuse Lyα more difficult. Indeed, a Lyα CGM halo was not detected in this quasar in a 0.8 hours exposure (Farina et al. 2019). However, PSOJ183+05 is being followed up with deeper observations as part of the MUSE program 112.262L.002 (PI E. Farina). In addition, upcoming Cycle 3 JWST observations with NIRSpec IFU (GO program 4912, PI S. Carniani) will allow us to map the morphology, metal enrichment and kinematics in the host-galaxy and up to the CGM of PSOJ183+05, using rest-frame optical tracers such as Hα λ6564 Å, [OIII] λ5008 Å, and other metal lines (Marshall et al. 2023; Liu et al. 2024; Decarli et al. 2024). Such an approach is key to build a detailed picture of how baryons cycle between galaxies and their CGM, and improve the current understanding of the evolution of the first massive galaxies.

Facilities: ALMA.

Software: astropy (Astropy Collaboration et al.
2013, 2018, 2022),

REFERENCES

Adelberger, K. L., Steidel, C. C., Pettini, M., et al. 2005, ApJ, 619, 697, doi: 10.1086/426580

Akins, H. B., Fujimoto, S., Finlator, K., et al. 2022, ApJ, 934, 64, doi: 10.3847/1538-4357/ac795b

Appleton, P. N., Guillard, P., Boulanger, F., et al. 2013, ApJ, 777, 66, doi: 10.1088/0004-637X/777/1/66

Astropy Collaboration, Robitaille, T. P., Tollerud, E. J., et al. 2013, A&A, 558, A33, doi: 10.1051/0004-6361/201322068

Astropy Collaboration, Price-Whelan, A. M., Sipőcz, B. M., et al. 2018, AJ, 156, 123, doi: 10.3847/1538-3881/aabc4f

Astropy Collaboration, Price-Whelan, A. M., Lim, P. L., et al. 2022, ApJ, 935, 167, doi: 10.3847/1538-4357/ac7c74

Bañados, E., Venemans, B. P., Decarli, R., et al. 2016, ApJS, 227, 11, doi: 10.3847/0067-0049/227/1/11

Barai, P., Gallerani, S., Pallottini, A., et al. 2018, MNRAS, 473, 4003, doi: 10.1093/mnras/stx2563

Bischetti, M., Maiolino, R., Carniani, S., et al. 2019a, A&A, 630, A59, doi: 10.1051/0004-6361/201833557

Bischetti, M., Piconcelli, E., Vietri, G., et al. 2017, A&A, 598, A122, doi: 10.1051/0004-6361/201629301

Bischetti, M., Piconcelli, E., Feruglio, C., et al. 2018, A&A, 617, A82, doi: 10.1051/0004-6361/201833249

—. 2019b, A&A, 628, A118, doi: 10.1051/0004-6361/201935524

Bischetti, M., Feruglio, C., Piconcelli, E., et al. 2021, A&A, 645, A33, doi: 10.1051/0004-6361/202039057

Bischetti, M., Choi, H., Fiore, F., et al. 2024, ApJ, 970, 9, doi: 10.3847/1538-4357/ad4a77

Borisova, E., Cantalupo, S., Lilly, S. J., et al. 2016, ApJ, 831, 39, doi: 10.3847/0004-637X/831/1/39

Butler, K. M., van der Werf, P. P., Topkaras, T., et al. 2023, ApJ, 949, 122, doi: 10.3847/1538-4357/acd453

Carniani, S., Ferrara, A., Maiolino, R., et al. 2020, MNRAS, 499, 5136, doi: 10.1093/mnras/staa3178

Casavecchia, B., Maio, U., Péroux, C., & Ciardi, B. 2024, A&A, 689, A106, doi: 10.1051/0004-6361/202450332

Cicone, C., Maiolino, R., Sturm, E., et al. 2014, A&A, 562, A21, doi: 10.1051/0004-6361/201322464

Cicone, C., Maiolino, R., Gallerani, S., et al. 2015, A&A, 574, A14, doi: 10.1051/0004-6361/201424980

Cicone, C., Mainieri, V., Circosta, C., et al. 2021, A&A, 654, L8, doi: 10.1051/0004-6361/202141611

Costa, T. 2023, arXiv e-prints, arXiv:2308.12987, doi: 10.48550/arXiv.2308.12987

Costa, T., Arrigoni Battaia, F., Farina, E. P., et al. 2022, MNRAS, 517, 1767, doi: 10.1093/mnras/stac2432

Costa, T., Rosdahl, J., & Kimm, T. 2019, MNRAS, 489, 5181, doi: 10.1093/mnras/stz2471

Decarli, R., Walter, F., Venemans, B. P., et al. 2018, ApJ, 854, 97, doi: 10.3847/1538-4357/aaa5aa

Decarli, R., Dotti, M., Bañados, E., et al. 2019, ApJ, 880, 157, doi: 10.3847/1538-4357/ab297f

Decarli, R., Pensabene, A., Diaz-Santos, T., et al. 2023, A&A, 673, A157, doi: 10.1051/0004-6361/202245674

Decarli, R., Loiacono, F., Farina, E. P., et al. 2024, A&A, 689, A219, doi: 10.1051/0004-6361/202449239

Ding, X., Onoue, M., Silverman, J. D., et al. 2023, Nature, 621, 51, doi: 10.1038/s41586-023-06345-5

Duras, F., Bongiorno, A., Piconcelli, E., et al. 2017, A&A, 604, A67, doi: 10.1051/0004-6361/201731052

Farina, E. P., Arrigoni-Battaia, F., Costa, T., et al. 2019, ApJ, 887, 196, doi: 10.3847/1538-4357/ab5847

Farina, E. P., Schindler, J.-T., Walter, F., et al. 2022, arXiv e-prints, arXiv:2207.05113. https://arxiv.org/abs/2207.05113

Feruglio, C., Ferrara, A., Bischetti, M., et al. 2017, A&A, 608, A30, doi: 10.1051/0004-6361/201731387

Feruglio, C., Fiore, F., Carniani, S., et al. 2018, A&A, 619, A39, doi: 10.1051/0004-6361/201833174

Fiore, F., Feruglio, C., Shankar, F., et al. 2017, A&A, 601, A143, doi: 10.1051/0004-6361/201629478

Fluetsch, A., Maiolino, R., Carniani, S., et al. 2019, MNRAS, 483, 4586, doi: 10.1093/mnras/sty3449

Förster Schreiber, N. M., Renzini, A., Mancini, C., et al. 2018, ApJS, 238, 21, doi: 10.3847/1538-4365/aadd49

Fudamoto, Y., Smit, R., Bowler, R. A. A., et al. 2022, ApJ, 934, 144, doi: 10.3847/1538-4357/ac7a47

Fujimoto, S., Ouchi, M., Ferrara, A., et al. 2019, ApJ, 887, 107, doi: 10.3847/1538-4357/ab480f

Fujimoto, S., Silverman, J. D., Bethermin, M., et al. 2020, ApJ, 900, 1, doi: 10.3847/1538-4357/ab94b3

Galbiati, M., Fumagalli, M., Fossati, M., et al. 2023, MNRAS, 524, 3474, doi: 10.1093/mnras/stad2087

Ginolfi, M., Jones, G. C., Béthermin, M., et al. 2020a, A&A, 643, A7, doi: 10.1051/0004-6361/202038284

—. 2020b, A&A, 643, A7, doi: 10.1051/0004-6361/202038284

Hailey-Dunsheath, S., Nikola, T., Stacey, G. J., et al. 2010, ApJL, 714, L162, doi: 10.1088/2041-8205/714/1/L162

Herrera-Camus, R., Förster Schreiber, N., Genzel, R., et al. 2021, A&A, 649, A31, doi: 10.1051/0004-6361/202039704

Inoue, S., Dekel, A., Mandelker, N., et al. 2016, MNRAS, 456, 2052, doi: 10.1093/mnras/stv2793

Izumi, T., Onoue, M., Matsuoka, Y., et al. 2021a, ApJ, 908, 235, doi: 10.3847/1538-4357/abd7ef

—. 2021b, ApJ, 908, 235, doi: 10.3847/1538-4357/abd7ef

Janssen, A. W., Christopher, N., Sturm, E., et al. 2016, ApJ, 822, 43, doi: 10.3847/0004-637X/822/1/43

Jones, G. C., Maiolino, R., Carniani, S., et al. 2023, MNRAS, 522, 275, doi: 10.1093/mnras/stad985

Kashino, D., Lilly, S. J., Matthee, J., et al. 2023, ApJ, 950, 66, doi: 10.3847/1538-4357/acc588

Lagache, G., Cousin, M., & Chatzikos, M. 2018, A&A, 609, A130, doi: 10.1051/0004-6361/201732019

Lambert, T. S., Posses, A., Aravena, M., et al. 2023, MNRAS, 518, 3183, doi: 10.1093/mnras/stac3016

Lamperti, I., Harrison, C. M., Mainieri, V., et al. 2021, A&A, 654, A90, doi: 10.1051/0004-6361/202141363

Liu, W., Fan, X., Yang, J., et al. 2024, ApJ, 976, 33, doi: 10.3847/1538-4357/ad7de4

Maiolino, R., Gallerani, S., Neri, R., et al. 2012, MNRAS, 425, L66, doi: 10.1111/j.1745-3933.2012.01303.x

Marshall, M. A., Perna, M., Willott, C. J., et al. 2023, A&A, 678, A191, doi: 10.1051/0004-6361/202346113

Mazzucchelli, C., Bischetti, M., D'Odorico, V., et al. 2023, A&A, 676, A71, doi: 10.1051/0004-6361/202346317

McMullin, J. P., Waters, B., Schiebel, D., Young, W., & Golap, K. 2007, in Astronomical Society of the Pacific Conference Series, Vol. 376, Astronomical Data Analysis Software and Systems XVI, ed. R. A. Shaw, F. Hill, & D. J. Bell, 127

Meyer, R. A., Walter, F., Cicone, C., et al. 2022, ApJ, 927, 152, doi: 10.3847/1538-4357/ac4e94

Neeleman, M., Walter, F., Decarli, R., et al. 2023, ApJ, 958, 132, doi: 10.3847/1538-4357/ad05d2

Neeleman, M., Novak, M., Venemans, B. P., et al. 2021, ApJ, 911, 141, doi: 10.3847/1538-4357/abe70f

Novak, M., Venemans, B. P., Walter, F., et al. 2020, ApJ, 904, 131, doi: 10.3847/1538-4357/abc33f

Obreja, A., Arrigoni Battaia, F., Macciò, A. V., & Buck, T. 2024, MNRAS, 527, 8078, doi: 10.1093/mnras/stad3410

Pizzati, E., Ferrara, A., Pallottini, A., et al. 2023, MNRAS, 519, 4608, doi: 10.1093/mnras/stac3816

Prochaska, J. X., Lau, M. W., & Hennawi, J. F. 2014, ApJ, 796, 140, doi: 10.1088/0004-637X/796/2/140

Scholtz, J., Maiolino, R., Jones, G. C., & Carniani, S. 2023, MNRAS, 519, 5246, doi: 10.1093/mnras/stac3787

Shimizu, T. T., Davies, R. I., Lutz, D., et al. 2019, MNRAS, 490, 5860, doi: 10.1093/mnras/stz2802

Solomon, P. M., & Vanden Bout, P. A. 2005, ARA&A, 43, 677, doi: 10.1146/annurev.astro.43.051804.102221

Springel, V., White, S. D. M., Jenkins, A., et al. 2005, Nature, 435, 629, doi: 10.1038/nature03597

Stern, J., Sternberg, A., Faucher-Giguère, C.-A., et al. 2021, MNRAS, 507, 2869, doi: 10.1093/mnras/stab2240

Stone, M. A., Lyu, J., Rieke, G. H., & Alberts, S. 2023, ApJ, 953, 180, doi: 10.3847/1538-4357/acebe0

Stone, M. A., Lyu, J., Rieke, G. H., Alberts, S., & Hainline, K. N. 2024, ApJ, 964, 90, doi: 10.3847/1538-4357/ad2a57

Tripodi, R., Feruglio, C., Fiore, F., et al. 2022, arXiv e-prints, arXiv:2207.03314. https://arxiv.org/abs/2207.03314

Tripodi, R., Scholtz, J., Maiolino, R., et al. 2024a, A&A, 682, A54, doi: 10.1051/0004-6361/202347081

Tripodi, R., Feruglio, C., Fiore, F., et al. 2024b, A&A, 689, A220, doi: 10.1051/0004-6361/202349054

Tumlinson, J., Peeples, M. S., & Werk, J. K. 2017, ARA&A, 55, 389, doi: 10.1146/annurev-astro-091916-055240

Turner, M. L., Schaye, J., Steidel, C. C., Rudie, G. C., & Strom, A. L. 2014, MNRAS, 445, 794, doi: 10.1093/mnras/stu1801

Valentini, M., Gallerani, S., & Ferrara, A. 2021, MNRAS, 507, 1, doi: 10.1093/mnras/stab1992

Vayner, A., Díaz-Santos, T., Eisenhardt, P. R. M., et al. 2024, arXiv e-prints, arXiv:2412.02862, doi: 10.48550/arXiv.2412.02862

Veilleux, S., Bolatto, A., Tombesi, F., et al. 2017, ApJ, 843, 18, doi: 10.3847/1538-4357/aa767d

Venemans, B. P., Neeleman, M., Walter, F., et al. 2019, ApJL, 874, L30, doi: 10.3847/2041-8213/ab11cc

Venemans, B. P., Walter, F., Neeleman, M., et al. 2020, ApJ, 904, 130, doi: 10.3847/1538-4357/abc563

Vito, F., Di Mascia, F., Gallerani, S., et al. 2022, MNRAS, 514, 1672, doi: 10.1093/mnras/stac1422

Wang, F., Yang, J., Fan, X., et al. 2024, ApJ, 968, 9, doi: 10.3847/1538-4357/ad3fb4

Yue, M., Eilers, A.-C., Simcoe, R. A., et al. 2024, ApJ, 966, 176, doi: 10.3847/1538-4357/ad3914

Zanchettin, M. V., Feruglio, C., Massardi, M., et al. 2023, A&A, 679, A88, doi: 10.1051/0004-6361/202245729

Zanella, A., Iani, E., Dessauges-Zavadsky, M., et al. 2024, A&A, 685, A80, doi: 10.1051/0004-6361/202349074